

Environmental Science Nano

Accepted Manuscript



This is an *Accepted Manuscript*, which has been through the Royal Society of Chemistry peer review process and has been accepted for publication.

Accepted Manuscripts are published online shortly after acceptance, before technical editing, formatting and proof reading. Using this free service, authors can make their results available to the community, in citable form, before we publish the edited article. We will replace this *Accepted Manuscript* with the edited and formatted *Advance Article* as soon as it is available.

You can find more information about *Accepted Manuscripts* in the [Information for Authors](#).

Please note that technical editing may introduce minor changes to the text and/or graphics, which may alter content. The journal's standard [Terms & Conditions](#) and the [Ethical guidelines](#) still apply. In no event shall the Royal Society of Chemistry be held responsible for any errors or omissions in this *Accepted Manuscript* or any consequences arising from the use of any information it contains.

The Ultra small size water soluble NAC-Qdot used in this study can be a taggant and delivery cargo inside the plant system. Its fluorescence property can help to track its localization inside the plant system. Fluorescence imaging technique has been used as an efficient tool. Along with this we have observed that it can be used as a nutrient medium to boost the germination and growth of snow pea plant (*Pisum sativum*). We believe our study can help and bring a new direction to research going on in the new emerging nano-agricultural studies.

Effect of N-Acetyl Cysteine Coated CdS:Mn/ZnS Quantum Dots on Seed Germination and Seedling Growth of Snow Pea (*Pisum sativum L.*): Imaging and Spectroscopic Studies

Authors: Smruti Das¹, Brandon P. Wolfson¹, Laurene Tetard^{1,2,3}, Jeremy Tharkur^{1,4}, Joshua Bazata^{1,4} and Swadeshmukul Santra^{1,3,4,5,*}

¹NanoScience Technology Center, ²Department of Physics, ³Department of Materials Science and Engineering, ⁴Burnett School of Biomedical Sciences, and ⁵Department of Chemistry, University of Central Florida, 12424 Research Parkway, Suite 400, Orlando, FL 32826.

*Corresponding author

Swadeshmukul Santra

NanoScience Technology Center, Department of Chemistry, Department of Materials Science and Engineering and Burnett School of Biomedical Sciences

University of Central Florida

12424 Research Parkway

Suite 400, Research Pavilion

Orlando, FL 32826, USA

Phone: 407-882-2848

Fax: 407-882-2819

E-mail: ssantra@mail.ucf.edu

ABSTRACT

Anthropogenic nanomaterials (ANMs), once produced, will inevitably be present in the environment. Depending on their environmental stability and level of toxicity, ANMs raise some concern regarding their potential impact on the surrounding animal, aquatic and plant life. In this study, we demonstrate for the first time the effect of ultra-small size (< 5 nm) semiconductor ANMs on the germination and growth of seeds of Snow Peas model plant system (*Pisum sativum*) using a N-Acetyl Cysteine (NAC) coated core-shell CdS:Mn/ZnS Qdots as a heavy metal ion containing model ANM. We present combined results of fluorescence confocal, Atomic Force Microscopy (AFM) and Raman imaging of Quantum dot (Qdot) to track the uptake and localization (translocation) in plant tissue. It was found that Qdots were localized on the surface seed coat, epidermis and intercellular regions. Germination, growth and chlorophyll content of the seedlings were found to be strongly dependent on Qdot dosage and time of seed incubation with Qdots. Interestingly, no acute Cd metal toxicity was observed while at Qdot concentration below $40\mu\text{g/mL}$, and seed germination and growth processes were promoted.

Keywords: Cadmium Sulfide, NAC, ZnS, Peas, Seed Germination

1. Introduction

Anthropogenic nanomaterials (ANMs) are a class of materials specifically engineered to exhibit unique physical and chemical properties at the nanoscale (size below 100 nm). After their useful life, ANMs are bound to interact with their environment, but their potential impact on animal, plant and aquatic life is not yet fully understood, thus potentially raising serious environmental concerns. ^[1] Studying the interaction of ANMs with the plant vascular system to assess their potential ecotoxicity in physiological conditions (*in vivo*) and understand ANM uptake by plant cells and tissues is therefore necessary, and calls for suitable imaging and spectroscopy techniques. In addition to nano- and microscopic interactions of ANMs with plants, their immediate phenotypic effects on seed germination and plant growth should be considered. Hence due to the intrinsic complexity of plants, several routes of nanoparticle exposure must be taken into account.

Some of these parameters have been examined in previous related studies. ^[2-11] As seed germination and vegetative phase are the two most important stages of plant growth, during which the plant is most sensitive to its different environmental conditions, various studies have considered tolerance, uptake and possible accumulation of environmental contaminants in roots and shoots, and the effect of nanoparticles (NPs) on seed germination and seedling growth. ^[2-12] Furthermore, a number of other parameters including particle size, surface charge, surface coating chemistry, aspect ratio, and composition of ANMs are expected to greatly affect the overall plant physiology. ^[3,4] An inhibitory effect of zinc oxide (ZnO) NPs (20 ± 5 nm) on corn seed germination at a concentration of 2000 ppm, root growth inhibition of 50 % at 50 ppm in radish, and at 20 ppm in rape and ryegrass plant systems has also been shown. ^[6] However another study reported beneficial effects on seed germination and seedling growth at 1000 ppm with 25 nm mean particle size, while inhibitory effect at higher concentration. ^[5] Priester et al. also considered the

translocation of ZnO NPs in plant tissues after soil application.^[7] The overall metal concentrations were increased in plant tissues as a result of the treatment, somewhat compromising food quality, but showing no toxicity.^[7] Similar treatments with CeO₂ NPs led to the plant nitrogen fixation process being shut down, and created negative ecotoxicological impact.^[13] The impact of NPs containing non-nutrient based metal ions such as silver (Ag) and gold (Au) on seed germination and plant growth has also been considered. Yin et al. reported an inhibitory effect of gum arabic coated Ag NPs on seed growth at 40 ppm, whereas no inhibitory effect was observed for polyvinylpyrrolidone coated Ag NPs and AgNO₃ salts, suggesting that phytotoxicity of Ag NPs is dependent on surface coating chemistry.^[8] Similar inhibitory effects of Ag NPs were also observed on rice seed germination and seedling growth with the increasing NP sizes and concentrations.^[11] However, Kumar et al. showed that Au NPs of 24 nm size induced vegetative growth and enhanced seed yield of *Arabidopsis thaliana* model plant system.^[5] Finally, carbon nanotubes did not exhibit any significant adverse impact on the plant growth.^[6] In fact, carbon nanotubes enhanced growth in tobacco plant cells.^[9]

One critical aspect to understand ANMs translocation and their ultimate fate in plant vascular systems and their effect of the overall behavior of the plant is the necessity to develop suitable imaging techniques capable of resolving nanoparticles signatures. Photoacoustic and photothermal based detection of carboneous nanomaterial were used to monitor the interaction of activated carbon, carbon nanotubes and graphene with tomato plant.^[10] However, the metrology available for such studies remains underexplored.

Herein we investigated the effect of ultra-small size (~5.0 nm) NAC-coated CdS:Mn/ZnS Qdots on the germination of seeds and seedling growth of snow peas (*P. sativum*). NAC is an antioxidant biomolecule as well as a water-soluble carboxylated (negatively-charged) capping agent for Qdots. We report fluorescence, atomic force microscopy (AFM) and Raman spectroscopy

based surface and chemical imaging investigation of the structural and content analysis of seeds to monitor possible nanoparticle-cell interaction inside plant cells resulting from Qdot treatments. The study was complemented by a physiological study of germination and growth parameters.

2. Materials and methods

2.1. Materials

All reagents were purchased from commercial vendors and used without any further purification unless stated specifically. Cadmium acetate dihydrate, manganese acetate tetrahydrate, N-acetyl-L-cysteine (NAC) and dioctyl sulfosuccinate sodium salt (Aerosol OT, AOT) were purchased from Acros Organics (New Jersey, US). Zinc acetate dihydrate and sodium sulfide was purchased from Sigma-Aldrich (St. Louis, MO). HPLC grade heptane and ethanol (95%; V/V) were obtained from Fisher Scientific (Pittsburgh, PA) and acetone was obtained from VWR (Radnor, PA). Purified deionized Water (DI) was obtained from Nanopure (Barnstead Nanopure Diamond purifier; model # D11931).

2.2. Synthesis of NAC Coated CdS:Mn/ZnS Qdots

CdS:Mn/ZnS Qdots were synthesized via a reverse micelle method following a published protocol [21,22] with some modifications as stated below. Three stock solutions (A, B and C) of salts (cadmium acetate dihydrate, manganese acetate, sodium sulfide, zinc acetate) were separately prepared. Stock solution “A” contains a mixture of 266 mg (0.1 mol) of cadmium acetate and 4.9 mg of manganese acetate (1.8 mol % with respect to metallic Cd) in 10 mL of DI water. Stock solution (5 mL; DI water) of “B” and “C” contain 257.5 mg of sodium sulfide and 285.3 mg of zinc acetate dehydrate (0.26 mol), respectively. Then three separate AOT/heptane/water water-in-oil (W/O) microemulsion solutions, 1, 2 and 3 were prepared containing 0.9 mL of stock solution “A”, 2.7 mL of stock solution “B” and 2.7 mL of stock solution “C”, respectively. Microemulsion

1 contains 2.23 g AOT and 25 mL heptane, whereas microemulsions 2 and 3 contain 6.69 g AOT and 75 mL heptane. Microemulsion 1 was added to 2 followed by magnetic stirring for 15 min. Thereafter microemulsion 3 was added to the combined mixture of 1 and 2 dropwise. After 24 hr of stirring, bright yellow-orange color emission was seen when the microemulsion solution was exposed to a hand-held UV lamp (Mineralight[®], multiband UV 254/365nm lamp, Model UVGL-58) confirming formation of CdS:Mn/ZnS Qdots. Post coating with NAC was done while Qdots were present in W/O microemulsion. NAC coating procedure involved the following steps. A W/O microemulsion containing NAC was prepared by combining 175 mL of heptane, 15.61 g AOT and 0.55 mg NAC solution (prepared in 6.3 mL of DI water). Next, NAC containing microemulsion was added dropwise to Qdot microemulsion followed by stirring 24 hr. NAC coated Qdots (NAC-Qdots) were then recovered by first destabilizing the microemulsion using a solvent mixture of acetone and ethanol (95% V/V) followed by centrifugation (11,000 rpm for 10 min). The NAC-Qdot pellet was then re-dispersed in 10 mL of acetone followed by centrifugation (11,000 rpm, 5 min), sonication (5 min) and vortexing (2-3 min). This washing procedure was repeated using acetone (2x), heptane (2x) and acetone (1x). Finally, the NAC-Qdot pellet was dried at 60 °C for 4 min to obtain the product in powder form.

2.3. UV-Visible and fluorescence spectroscopy

All UV-Visible absorption and fluorescence emission spectra were recorded at room temperature using a Cary 300 UV-VIS Spectrophotometer and a NanoLog Spectrofluorimeter (SPEX, Jobin Yvon Horiba), respectively. A quartz cuvette (1cm path length) was used for all UV-Vis and fluorescence measurements. For UV-Vis measurements, the instrument was calibrated against DI water in the wavelength range 200 – 800 nm. 450 µl of a stock solution of 1 mg/ml NAC-Qdot diluted with 2 ml of DI water was used to take the OD. Fluorescence emission

spectrum was recorded at 375 nm excitation keeping slit width (both excitation and emission) fixed at 5 nm and scan rate at 1nm/sec.

2.4. High resolution transmission electron microscopy (HRTEM)

Characterization of Qdot crystal size and crystallinity was performed using a FEI Technai F30 High-Resolution Transmission Electron Microscopy (HRTEM). Carbon coated copper grids with 400 mesh (Electron Microscopy Sciences) were submerged in NAC-Qdot solution (in DI water) for 20-30 min and then placed on absorbing task wipers (Kimwipes, Kimtech Science brand; Kimberly-Clark) in a plastic petri dish to dry overnight. Grids were transported for HRTEM analysis for measuring crystal size and visualizing the crystallinity.

2.5. Preparation of seeds and plant growth condition

Snow Pea (*P. sativum*) seeds were purchased from Lucas Nursery, Orlando, FL and stored in a dry opaque packet at room temperature. Prior to use, seeds were soaked in DI water for 30 min to soften the seed coat. Thereafter surface sterilization was performed by washing the seeds with separate solutions of 70% ethanol and 1% sodium hypochlorite for 1 minute. Seeds were then washed five times with DI water to ensure the removal of additional sterilizing solutions remaining on the surface. The sets of Qdot treated and untreated seeds were sown in cups containing potting mixture at a constant day/night temperature (70/65°F) to see the effect of Qdot on seedling growth (roots and shoots length).

2.6. Plant germination tests

Exposure of plant cells to excess amount of Qdots could raise ROS level (i.e. beyond a maximum tolerable dose) which could negatively impact plant genotype. To test this hypothesis, we investigated the effect of different concentrations of NAC-Qdot on seed germination, root length, shoot length and chlorophyll content of snow pea genotype. Different concentrations of NAC-

Qdots (0, 2, 5, 10, 20, 40, 60, 80, 100 $\mu\text{g/mL}$) were prepared in DI water to study their effect on seed germination and growth of seedling of snow pea (*P. sativum*). Seeds were soaked under different concentrations of freshly prepared NAC-Qdot for 24 hr. Seed germination was tested on moist filter paper (WhatmanTM filter paper size 41; GE Healthcare Life sciences). In each Petri dish (85 mm diameter), 20 seeds were randomly placed on the filter paper, then 5 mL of NAC-Qdot solution was added (i.e. treated seed samples). The controls were maintained by similarly treating seeds with 5 mL of DI water. Seeds were germinated for five days under dark in a controlled environmental condition (25 °C and 50% Relative Humidity, RH). Germination was considered successful when the coleoptiles were longer than 2 mm. Three replicates were carried out for each treatment. Germination rate is the average number of seeds that germinate over the five-day time period.

$$\text{Germination}(\%) = \frac{\text{Number of seeds germinated}}{\text{Total number of seeds in petri dish}} \times 100\%$$

2.7. Chlorophyll estimation

Leaves were collected from 15 day old seedling to estimate chlorophyll content. Freshly cut leaves (40 mg) were weighed and put in 80% acetone for chlorophyll estimation. Chlorophyll a, chlorophyll b and total chlorophyll were estimated following Arnon's method using the specific absorption coefficient given by Mackinney in 1941.^[23,24] The Optical Density (OD values) of the solutions was read at 645 and 663 nm using a SpectraMax 190 absorbance plate reader equipped with SoftMax® ProData acquisition & analysis software.

$$\text{Chlorophyll a (mg g}^{-1}\text{)} = (12.7(\text{OD}_{663}) - 2.69(\text{OD}_{645})) \frac{V}{1000 \times w}$$

$$\text{Chlorophyll } b \text{ (mg g}^{-1}\text{)} = (22.9(OD_{645}) - 4.68(OD_{663})) \frac{V}{1000 \times w}$$

$$\text{Total Chlorophyll (mg g}^{-1}\text{)} = (20.2(OD_{645}) + 8.02(OD_{663}))$$

where $OD = \text{OpticalDensity}$

$V = \text{Final volume of 80\% acetone (i. e. 25 ml)}$

$w = \text{Dry weight of sample taken (i. e. 40 mg)}$

2.8. Sample preparation for microscopy

For the microscopic studies, cross sections ($\sim 300 \mu\text{m}$ thick slice) of treated and untreated seeds without seed coats (cotyledons) were prepared manually using a single edge blade ($\sim 230 \mu\text{m}$ thickness; American Safety Razor Company; Catalogue # 66-0392; Verona, VA) and mounted on microscope slides (Fisherbrand[®]; Size 12x75x1 mm; Catalogue # 12-550-003).

Confocal and phase contrast microscopy: Samples were characterized under phase contrast (Olympus 1X71, Japan) and laser scanning confocal microscope (Olympus BX51 Fluoview). Phase contrast microscopy was acquired using excitation filter of 360/40 nm with a dichroic mirror of ZT365bcm and the emission filter used was 585/20nm. Stacks of confocal images were collected (in Z-stack sections; 1 image at an interval of 1 μm scan depth) and processed using ImageJ software (National Institutes of Health). The presence of Qdots was detected either by differential interference contrast or reflection. For the latter, the specimens were excited with laser line of 405nm (Olympus LD 405) and the reflected signal was collected in the range of 510 long pass emission.

2.9. Raman spectroscopy

Raman spectroscopy measurements were performed on Witec alpha300 RA under ambient conditions with excitation wavelength of 532 nm and using a Zeiss 20x objective. A full Raman

spectrum was collected at each point of the image with a 600g/mm grating, and integration time of 0.05 s. The Raman intensity and peak position maps were reconstructed using the data analysis toolbox available in the Witec Project Plus software.

2.10. Atomic force microscopy

Atomic force microscopy (AFM) images were obtained in tapping (AC) mode on Witec alpha300 RA under ambient conditions with standard cantilever (Al coating, $f_{\text{res}}=247$ kHz).

2.11. Statistical analysis

Each treatment was conducted with three replicates, and the results were presented as mean \pm SD (standard deviation). The statistical analysis of experimental data utilized the PASW Statistics 18 (IBM SPSS). Tukey's least significant difference (LSD) was used to compare each of the experimental value to its corresponding control at a significance level of $P < 0.05$.

3. Results and Discussion

3.1. Characterization of NAC-Qdot

HRTEM images of NAC-Qdots are shown in Figure 1a. Despite a few clusters, Qdots (dark contrast) were fairly monodispersed as seen in the low-magnification image (Figure 1a (i)). Average particle size was estimated around 5 nm based on individual measurements of 21 particles using ImageJ, is shown in the histogram (Figure 1 a(ii)). High magnification HRTEM imaging revealed crystal lattice planes 101 and 110 for CdS and ZnS, respectively (Figure 1A (iii)), with the corresponding electron diffraction pattern indicating Qdot crystallinity. HRTEM, therefore confirmed that the Qdot surface coating with NAC did not compromise the particles crystallinity (Figure 1a (iv)). Next, we performed comprehensive characterization of NAC and Qdots with UV-Vis, Fluorescence, and FTIR spectroscopy. The results are of great importance in order to track the NPs in the plant, and understand how their potential interactions with the plant tissues can affect their intrinsic properties. UV-visible spectra show an absorption peak of NAC around 225 nm, which was not present in the NAC-Qdot

spectrum. However, the NAC-Qdot compound exhibits an absorption peak of 320 nm (Figure 1b). Bare Qdot shows a typical absorption characteristics of a semiconductor material with no clear band maximum, rather a shoulder appeared around 250 nm which is considered as the Qdot absorption peak. This absorption peak is red shifted by about 70 nm once Qdot surface is conjugated to NAC. The shift in Qdot absorption is attributed to the formation of surface-related defects during chemical conjugation of NAC to Qdot surface. The absence of 225 nm NAC absorption peak could not be resolved in NAC-Qdot absorption spectrum as it was suppressed by the strong Qdot absorption in the 225 nm region. The fluorescence intensity of the Qdot and NAC-Qdot was observed at 590 nm, the peak emission wavelength, whereas NAC presented no fluorescence. The fluorescence of the Qdots is attributed to the Mn dopant (${}^4T_1 \Rightarrow {}^6A_1$ transition). The results show that the presence of NAC on the surface did not alter the Qdot emission properties. The bright yellow-orange fluorescence of the NAC-Qdot solution can be seen in the inset (Figure 1c). The strong Qdot fluorescence can be used as a powerful biomarker to uncover its uptake by plant cells. ^[14] These results were used to select appropriate filters in fluorescence imaging to detect NAC-Qdot in plant cells. Next, FTIR signatures of NAC, NAC-Qdot and bare Qdot were compiled (Figure 1d). The characteristic NAC S-H peak at 2552 cm^{-1} was not observed in NAC-Qdot, indicating chemical conjugation of NAC to the Qdot surface through the formation of Zn-S bonds. NAC is highly water soluble in a wide pH range (2.4 - 12.0) due to the presence of hydrophilic carboxyl ($-\text{COOH}$) and acetamide ($-\text{NHCOCH}_3$) groups. These hydrophilic groups are available in the NAC-Qdot composite as NAC is conjugated to Qdot surface through thiol (S-H) group. Therefore, NAC-Qdot exhibits excellent water solubility, as also reported by Zhao et al. ^[15]

3.2. Effect on seed germination

We then studied the effect of the ultra-small size (~ 5.0 nm) NAC-Qdots on the germination of seeds and seedling growth of snow Peas (*P. sativum*). A schematic diagram represents different

possibilities of NAC-Qdot impact on snow pea seed germination and seedling growth (Figure 2). When entering a plant, external agents can trigger reactive oxygen species (ROS) production, leading to oxidative stress resulting in antioxidant enzymes production.^[16] Qdot, being an external agent, is therefore expected to trigger antioxidant enzymes production, leading to enhanced nutrient uptake and metabolism. This might lead to change in physiological activities in plant system.

Physiological changes in seed germination against treatments of different concentrations for NAC-Qdots were observed (Table S1). Seed germination reached 100% within 48 hours under NAC-Qdot exposure. The radicle and coleoptile exhibited signs of enhanced growth for treatments up to 40µg/mL NAC-Qdot concentration, despite the presence of toxic Cd ions in NAC-Qdot (Figure 3a). Enhanced nitrogen assimilation^[17] and reduction in free radical production^[18,19] are considered to be possible contributing factors towards enhancement of seed germination. Interestingly, inhibition of the seed germination and seedling growth was clearly noticed for all treatments above the 40µg/mL NAC-Qdot concentration. To further understand the role of Qdot surface chemicals i.e. NAC and ZnS shell which protects the CdS core (Figure 3), the effect of each individual component of NAC-Qdot on seed germination was tested. These chemical components include NAC, zinc acetate, zinc acetate-NAC (1:1 molar ratio), cadmium acetate, sodium sulfide, AOT and DI water (control). Only soluble form of Qdot components were used as controls. We could not involve other possible controls such as CdS and ZnS particles due to their aqueous insolubility. Seeds were allowed to germinate over 5 days and observed that NAC (vi), zinc acetate (iii), and zinc acetate-NAC (ii) accelerated germination rate, as seen by the increase of radical length over time (Figure 3b). However, cadmium acetate (iv), sodium sulfide (v) and AOT (vii) completely suppressed growth (Figure3b). NAC is considered a free radical scavenger and is capable of reducing cellular toxicity induced by free-radicals.^[2] Heavy metal ions such as

Cadmium (Cd) ions are known to be cytotoxic because of their ability to produce free radicals. Cd transport from plant roots to above ground tissues has been observed and suggests possible threats to human health.^[17] Cd accumulation in plants is regulated by several physiological processes, including uptake from soil (via roots) and atmosphere (via shoots), resulting in xylem transport from root to shoot and phloem movement into grain during maturation.^[19] Its high phytotoxicity associated with uptake and accumulation in plants can influence plant growth.^[18,20] Under most environmental conditions, it has been shown that Cd causes damage after its uptake by the roots, which in turn reduces the absorption and affects the transport of nitrate from roots to shoots, by inhibiting the nitrate reductase activity in the shoots.^[21] Cd-induced deficiencies in Fe (II) have also been reported to severely affect photosynthesis.^[22] In our study we have used core-shell CdS:Mn/ZnS where the CdS crystalline core is protected by a wide band-gap ZnS semiconductor material. The ZnS shell not only stabilizes the CdS core from oxidation but minimizes release of free Cd ions. Furthermore, the Qdot surface capping agent, NAC, is expected to passivate any Cd toxicity through scavenging free radicals generated by the Qdot core. Enhancement in seed germination and seedling growth for NAC-Qdot treated seeds below 40 μ g/mL is therefore attributed to the combined effect of NAC and ZnS. Photographs of NAC-Qdot treated and untreated control seeds were illuminated using a handheld 366 nm multi-band UV excitation source (Figure 3c, d). A bright glow was observed from radicals of NAC-Qdot treated seeds in comparison to the radicals of the control seeds, which we believe to be due to the combined emission of Qdot and plant tissue auto-fluorescence. This indicates the uptake of Qdots by the seed and their systemic distribution in plant cells. Some radicals however appeared brighter than others, which could be due to non-uniform distribution of Qdots.

3.3. Raman spectroscopy, AFM and fluorescent microscopic studies

For these measurements, slices of the treated seed (about 5 mm diameter) were sectioned ~3-4 mm beneath the seed surface and then mounted on a microscope slides for imaging. To explore the NAC-Qdot content with higher spatial resolution, we performed Raman spectroscopy mapping and AFM. The Raman signatures in the epidermis and inner region of the seed suggest a non-homogeneous distribution of the nanoparticles in the tissue of the treated seeds (Figure 4). We first acquired an optical image of the seed (Figure 4a), and determined the region of interest (red box in Figure 4a) for analysis with the confocal Raman system (Figure 4b, c). Due to the fluorescence of the samples resulting from the excitation wavelength of 532 nm of the Raman system, we used the variations in the fluorescence background of the Raman spectra to probe the changes in nanoparticle distribution across the section of the seed. Raman spectra were collected every 500 nm to cover the area of the selected region (Figure 4b, c). The resulting data set displayed the position of the fluorescence peak at each point in Figure 4c. As can be seen in the scale bar, the position of the maximum peak varied from 655 cm^{-1} to 3125 cm^{-1} . For comparison, we present the characteristic signature of the pure NAC-Qdot solution (solid blue curve) in Figure 4f. For the NAC-Qdot solution, the fluorescence signature presented a characteristic peak around 3125 cm^{-1} , which was not observed in non-treated seed cross section. Hence the map presented in Figure 4c is a good indicator of the presence of NAC-Qdot in the tissue. To illustrate this, we presented two representative Raman spectra in Figure 4f. Locations labeled A and B in Figure 4c correspond to a maximum peak at 3125 cm^{-1} and 200 cm^{-1} respectively. As shown in Figure 4f, the spectrum acquired at point A clearly resembles the signature of the NAC-Qdots. Thus, a position of the peak maximum around $\sim 3100\text{ cm}^{-1}$ is likely linked to the presence of NAC-Qdots, as the fluorescence background of untreated pea tissue is similar to the one obtained in point B (Figure 4c). Hence suggesting the presence of NAC-Qdots in the seed, with high concentration in the bright (yellow)

regions of the map presented in Figure 4c. Despite the important chemical information provided by Raman spectroscopy in Figure 4b,c,f, the need for nanoscale imaging tools to precisely determine the organization of the nanoparticles in the plant tissue clearly emerges. Imaging plant tissues with high resolution is quite challenging. Thus, we performed AFM imaging at a location where a peak around 3100cm^{-1} was found in the Raman spectrum. The resulting AFM image (Figure 4e) revealed nanoparticle-like structures in the tissue. Such nanoscale structures were not present in other areas of the section. However, AFM only provides topographical information, and the composition of the features can only be accessed by Raman spectroscopy with lower spatial resolution. This constitutes a known limitation of current nanometrology tools, and will be the subject of further studies. Nonetheless, given that the Raman spectra indicate the presence of nanoparticles and that the AFM images clearly show nanoscale particles at the same location, our data suggest that the particles indeed correspond to the NAC-Qdots. The image shows possible signs of aggregation (inset in Figure 4e) surrounded with well dispersed nanoparticles inside the tissue. Beyond confirmation of the presence of the Qdot in the section, we used confocal and phase contrast microscopy to localize NAC-Qdot in the treated seeds. Confocal fluorescence images were acquired $\sim 1\text{mm}$ beneath the cotyledon surface. A stack of 20 images were collected in Z-direction of the sectioned tissue to localize the presence of any NAC-Qdot in the surrounding of the cells. Phase contrast images (Figure 5) in transmission (i) and fluorescence (ii) mode. Presence of NAC-Qdots in the seeds is shown by overlay of the phase contrast images with false blue-color transmission background and red color fluorescence of the NAC-Qdots (Figure 5iii). Interestingly, Qdots were mostly populated in the intracellular regions and the cell walls (red colored areas), and no sign of fluorescence could be found inside the cells. The same cotyledon section was then imaged using confocal microscope to find the location of NAC-Qdots. An overlay of confocal images (DIC and fluorescence images) is also shown (Figure 5iv). The DIC images (Figure 5)

represent a layer about 10 μm below the top surface of the sectioned tissue sample. The fluorescence signature of NAC-Qdot in the intracellular regions is evident as shown by false red color. Thus, this multi-prong microscopy study suggests that NAC-Qdots, with sizes around 5 nm, are small enough to penetrate the seed coat and reach the pith (i.e. about 2-3 mm beneath the cotyledon surface), while remaining in the intracellular region of the tissue. These findings suggest that NAC-Qdot migration to other plant parts including stems and leaves during the growth of the plant should be considered.

3.4. Physiological impact of NAC-Qdot on plants

Finally, to evaluate the impact of NAC-Qdot dosage during seed germination on seedling growth, we have measured root and shoot length of pea (*P. sativum*) seedlings. Seeds were exposed to different treatments for 48 hours followed by sowing in cups for 15 days. An average length of root and shoot at day 15 versus NAC-Qdot concentrations ranging from 0 to 100 $\mu\text{g/mL}$ has been plotted to represent the changes occurring at different treatment (Figure 6a). Several interesting behaviors could be observed from these plots. First, NAC-Qdot dosage affects the growth of shoots and roots non-linearly, where a solution of NAC-Qdot with concentration above 5 $\mu\text{g/mL}$ can induce shoot and root growth. The roots exhibited a significant increase in length from about 19 cm long in control plants to an average of 22 cm for treatments concentration ranging from 5 to 40 $\mu\text{g/mL}$. However no significant change in length was observed in roots and shoots lengths for treatment concentrations between 10 $\mu\text{g/mL}$ and 40 $\mu\text{g/mL}$. Above the 40 $\mu\text{g/mL}$ NAC-Qdot concentration, a close to linear decrease in shoots and roots length was observed. Interestingly, root growth was sharply inhibited (about 5 cm decrease per additional 20 $\mu\text{g/mL}$) in comparison to shoot growth (about 1 cm decrease per additional 20 $\mu\text{g/mL}$) above the 40 $\mu\text{g/mL}$ of NAC-Qdot concentration threshold. The effect on root and shoot length was statistically significant at $P < 0.05$ (Table S1). While the longest root (22.8 cm) was observed for the of 20 $\mu\text{g/mL}$ group, the shortest

root (9.1 cm) was recorded at 100 $\mu\text{g}/\text{mL}$ treatment. Shoot length of the three pea seedlings ranged from 27.9 to 34.1 cm and the variety, concentration and interactions of variety-concentration were found to be significant at 0.1% confidence level (Table S1). Similarly the shortest shoot lengths were seen at a 100 $\mu\text{g}/\text{mL}$ concentration (27.9 cm), on the other hand the highest shoot length was obtained at 10 $\mu\text{g}/\text{mL}$ (34.1 cm) of NAC-Qdot (Figure 6a). Thus, the initial boost in seedling growth reflected in the increase in root and shoot length is attributed to NAC-Qdot treatment followed by antioxidant enzymes production to suppress the ROS activity. It can then be inferred that antioxidant enzymes along with plant growth regulators involved in cell division and cell elongation, such as cytokinins and gibberellins, facilitate the plant growth.^[20] However, the difference in effect on the shoot and roots suggest a different distribution of the NAC-Qdot throughout the plant, and a higher impact of the treatment on the root activity. We surmise that the release of NAC and Zn from the shell of NAC-Qdot over time could be another contributing factor to the nutrient mediated root and shoot growth. Between 10 $\mu\text{g}/\text{mL}$ and 40 $\mu\text{g}/\text{mL}$ concentration, we believe that NAC and Zn induced increase in growth process is partially countered by the Cd ion induced phytotoxicity. Above 40 $\mu\text{g}/\text{mL}$ of NAC-Qdot concentration, Cd ion induced phytotoxicity becomes prominent causing overall decline in seedling growth. At the highest NAC-Qdot concentration, the possibility of particulate aggregation and deposition in plant vascular system could also contribute to seedling growth inhibition. Chlorophyll content in plant leaves is one of the contributing factors to assess the level of phytotoxicity. Therefore, in addition to the shoot and root length, the effect of increasing of NAC-Qdot concentration on the chlorophyll content of snow pea (*P. sativum*) seedling was considered. Average chlorophyll content (chlorophyll a, chlorophyll b and total chlorophyll) with respect to NAC-Qdot is also plotted at concentrations ranging from 0 to 100 $\mu\text{g}/\text{mL}$ (Figure 6b). A significant increase ($P < 0.05$) in chlorophyll a and total chlorophyll (a+b) content was observed in seedlings treated with solution

concentration ranging from 5 to 40 $\mu\text{g}/\text{mL}$ (Table S1 & Figure 6b). An increase in chlorophyll b content between 5 and 10 $\mu\text{g}/\text{mL}$ was also measured. Chlorophyll a and total chlorophyll (a+b) content were highest at 20 $\mu\text{g}/\text{mL}$ NAC-Qdot concentration and the estimated values were 1.058 and 1.357 mg per Gram Fresh Weight; $\text{mg G}^{-1}\text{FW}$, respectively. The lowest value of Chlorophyll a content (0.551 $\text{mg G}^{-1}\text{FW}$) was found at 100 $\mu\text{g}/\text{mL}$ while the lowest value of total chlorophyll (a+b) content (0.857 $\text{mg G}^{-1}\text{FW}$) was at 80 $\mu\text{g}/\text{mL}$ NAC-Qdot concentration. Chlorophyll b content was highest (0.384 $\text{mg per G}^{-1}\text{FW}$) at 10 $\mu\text{g}/\text{mL}$ and lowest (0.290 $\text{mg G}^{-1}\text{FW}$) at after treatment with the 2 $\mu\text{g}/\text{mL}$ NAC-Qdot concentration. As chlorophyll a and chlorophyll b are the pigments present inside chloroplast, help in absorbing light energy to synthesize glucose, an increase in chlorophyll content contributes to an enrichment of the photosynthetic rate, hence potentially leading to an increased amount of nutrient synthesis. In the present study, NAC-Qdot dosage above 40 $\mu\text{g}/\text{mL}$ exhibited negative impact on Chlorophyll a and total chlorophyll (a+b) content, indicating a probable disruption of the normal photosynthetic process. This is again attributed to Cd ion related phytotoxicity as described previously.

4. Conclusion

We investigated, for the first time, the impact of ultra-small size ($\sim 5\text{nm}$) NAC coated CdS:Mn/ZnS Qdot on seed germination and seedling growth on a Snow Pea (*P. sativum*) model system. The fluorescence of NAC-Qdot constituted an important marker to track the dispersion of the particulates in the seeds during germination, and for higher resolution microscopy. Upon 48 hours of exposure of seeds to NAC-Qdots, it was found that the Qdots had translocated a few cell layers beneath the seed surface as revealed from fluorescence and Raman imaging studies. The NAC-Qdots were found to accumulate in the inter-cellular region of the plant tissues. Interestingly, our results show a great influence of the NAC-Qdot dosage on seed germination and seedling growth patterns. Surface coating agents, NAC and Zn ions (of the Qdot ZnS shell) appeared to

passivate Cd ion related phytotoxicity (of the Qdot core) for NAC-Qdot concentration up to 40 $\mu\text{g/mL}$ concentration, which was identified as the threshold above which toxicity mechanisms take place in the snow pea plants. Above this threshold, drastic reduction in seedling growth was observed as well as negative impact on total Chlorophyll content (a+b). The molecular mechanisms of dose dependence of NAC-Qdot will be the focus of further studies.

Acknowledgement

Authors acknowledge in kind support from Mona Doshi and Dr. Andre Gesquiere (UCF NanoScience Technology Center, Department of Chemistry and CREOL College of Optics and Photonics) for fluorescence and phase contrast microscopy. Authors acknowledge in kind support from Dr. Helge Heinrich (UCF Department of Physics) with HRTEM. Authors also acknowledge UCF-Advanced Materials Processing and Analysis Center (AMPAC)-Materials Characterization Facility (MCF) for the electron microscopy facility. This research is partially supported by the National Science Foundation (NSF-CBET Grant Number 1159500) and the Citrus Research and Development Foundation, Inc. (Project # 907).

References

- 1 M. J. McCall, *Nat. Nanotechnol.* **2011**, *6*, 613–614.
- 2 Y. X. Chen, Y. F. He, Y. M. Luo, Y. L. Yu, Q. Lin, M. H. Wong, *Chemosphere* **2003**, *50*, 789–793.
- 3 R. Nair, S. H. Varghese, B. G. Nair, T. Maekawa, Y. Yoshida, D. S. Kumar, *Plant Sci.* **2010**, *179*, 154–163.
- 4 T. Yadav, A. A. Mungray, A. K. Mungray, *Rev. Environ. Contam. Toxicol.* **2014**, *230*, 83–110.

- 5 T. N. V. K. V Prasad, P. Sudhakar, Y. Sreenivasulu, P. Latha, V. Munaswamy, K. R. Reddy, T. S. Sreepasad, P. R. Sajanlal, T. Pradeep, *J. Plant Nutr.* **2012**, *35*, 905–927.
- 6 D. H. Lin, B. S. Xing, *Environ. Pollut.* **2007**, *150*, 243–250.
- 7 J. H. Priester, Y. Ge, R. E. Mielke, A. M. Horst, S. C. Moritz, K. Espinosa, J. Gelb, S. L. Walker, R. M. Nisbet, Y.-J. An, J. P. Schimel, R. G. Palmer, J. A. Hernandez-Viezcas, L. Zhao, J. L. Gardea-Torresdey, P. A. Holden, *Proc. Natl. Acad. Sci. U. S. A.* **2012**, *109*, E2451–E2456.
- 8 L. Yin, B. P. Colman, B. M. McGill, J. P. Wright, E. S. Bernhardt, *PLoS One* **2012**, *7*.
- 9 M. V Khodakovskaya, K. de Silva, A. S. Biris, E. Dervishi, H. Villagarcia, *ACS Nano* **2012**, *6*, 2128–2135.
- 10 M. V Khodakovskaya, K. de Silva, D. A. Nedosekin, E. Dervishi, A. S. Biris, E. V Shashkov, E. I. Galanzha, V. P. Zharov, *Proc. Natl. Acad. Sci. U. S. A.* **2011**, *108*, 1028–1033.
- 11 P. Thuesombat, S. Hannongbua, S. Akasit, S. Chadchawan, *Ecotoxicol. Environ. Saf.* **2014**, *104*, 302–309.
- 12 Z. W. Rang, S. V. K. Jagadish, Q. M. Zhou, P. Q. Craufurd, S. Heuer, *Environ. Exp. Bot.* **2011**, *70*, 58–65.
- 13 S. Bandyopadhyay, J. R. Peralta-Videa, G. Plascencia-Villa, M. José-Yacamán, J. L. Gardea-Torresdey, *J. Hazard. Mater.* **2012**, *241-242*, 379–86.
- 14 S. Pathak, E. Cao, M. C. Davidson, S. Jin, G. A. Silva, *J. Neurosci.* **2006**, *26*, 1893–1895.
- 15 D. Zhao, Z. He, W. H. Chan, M. M. F. Choi, *J. Phys. Chem. C* **2009**, *113*, 1293–1300.
- 16 S. Das, P. Krishnan, M. Nayak, *Expl Agric.* **2013**, *49*, 53–73.
- 17 Yang F, Hong F, You W, Liu C, Gao F, Wu C, P. Yang, *Biol Trace Elem Res* **2006**, *110*, 179–190.
- 18 Barba-Espin G, Diaz-Vivancos P, C.-M. MJ, *Plant Cell Environ.* **2010**, *33*, 981–994.
- 19 Hong F, Zhou J, Liu C, Yang F, Wu C, Zheng L, P. Yang, *Biol Trace Elem.* **2005**, *105*.
- 20 D. Stampoulis, S. K. Sinha, J. C. White, *Environ. Sci. Technol.* **2009**, *43*, 9473–9.
- 21 S. Santra, H. S. Yang, P. H. Holloway, J. T. Stanley, R. A. Mericle, *J. Am. Chem. Soc.* **2005**, *127*, 1656–1657.

- 22 S. Santra, H. Yang, J. T. Stanley, P. H. Holloway, B. M. Moudgil, G. Walter, R. A. Mericle, *Chem. Commun.* **2005**, 3144–3146.
- 23 D. I. Arnon, *Plant Physiol.* **1949**, *24*, 1–15.
- 24 G. Mackinney, *J. Biol. Chem* **1941**, *140*, 315–322.

FIGURES

Figure 1.

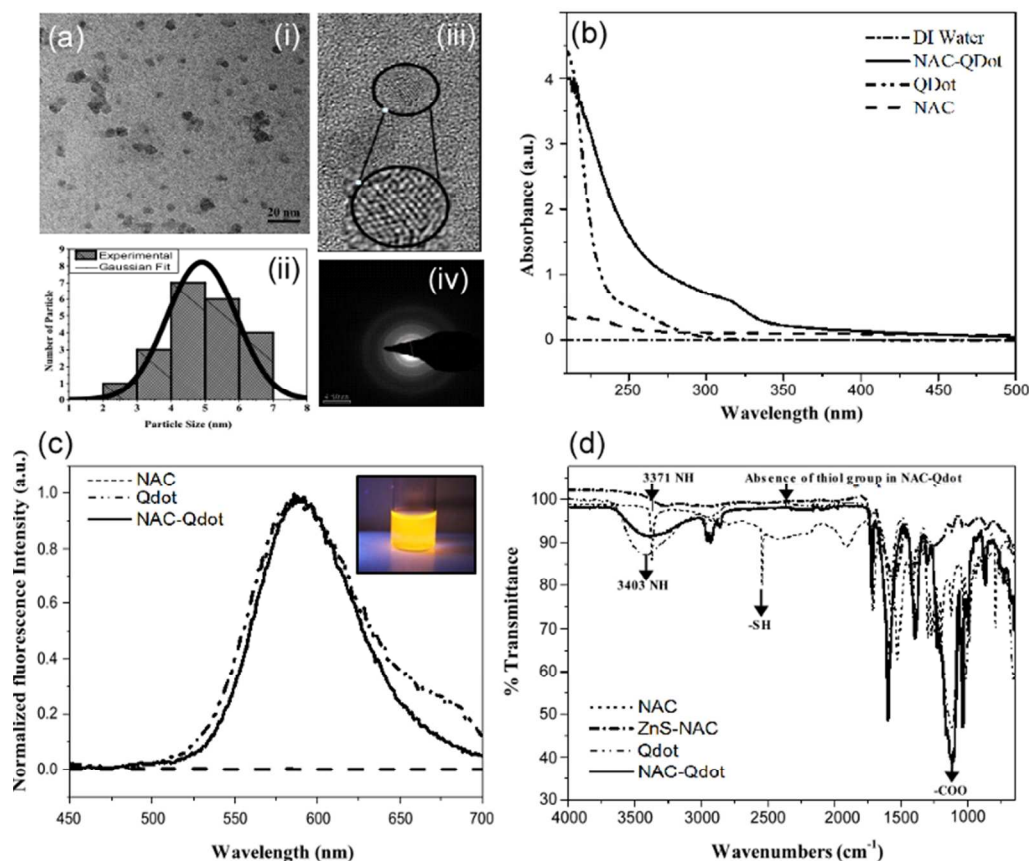


Figure 1. Characterization of NAC-Qdot. (a) HRTEM of NAC-Qdots; (i) low magnification image showing scattered dark contrast confirming the presence of electron-rich material (an inset shows) and (ii) histogram of particle size distribution, (iii) high magnification image showing crystalline lattice plane (lower-right inset), and (iv) selected area electron diffraction (SAED) pattern. (b) UV-Vis and (c) steady-state fluorescence emission spectra of NAC, bare Qdot and NAC-Qdot. Inset (top-left) is a digital image of glass vial containing NAC-Qdot solution in DI water showing characteristic bright orange-yellow emission when exposed to a hand-held 366 nm multiband UV excitation source and (d) FT-IR spectra of NAC, bare Qdot and NAC-Qdot.

Figure 2.

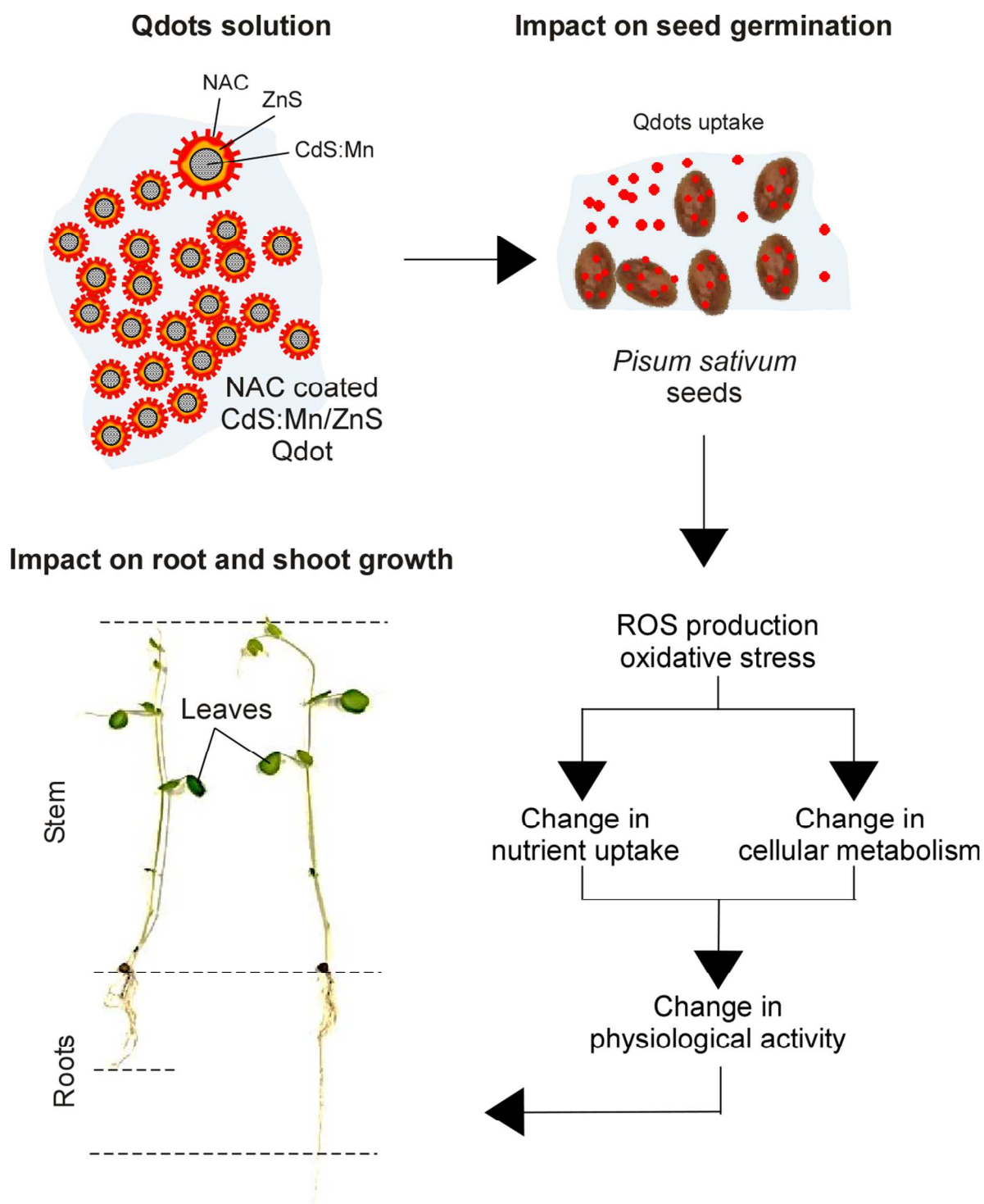


Figure 2. Schematic representation of possible effect of NAC-Qdot on seed germination and plant growth of snow pea (*Pisum sativum*)

Figure 3.

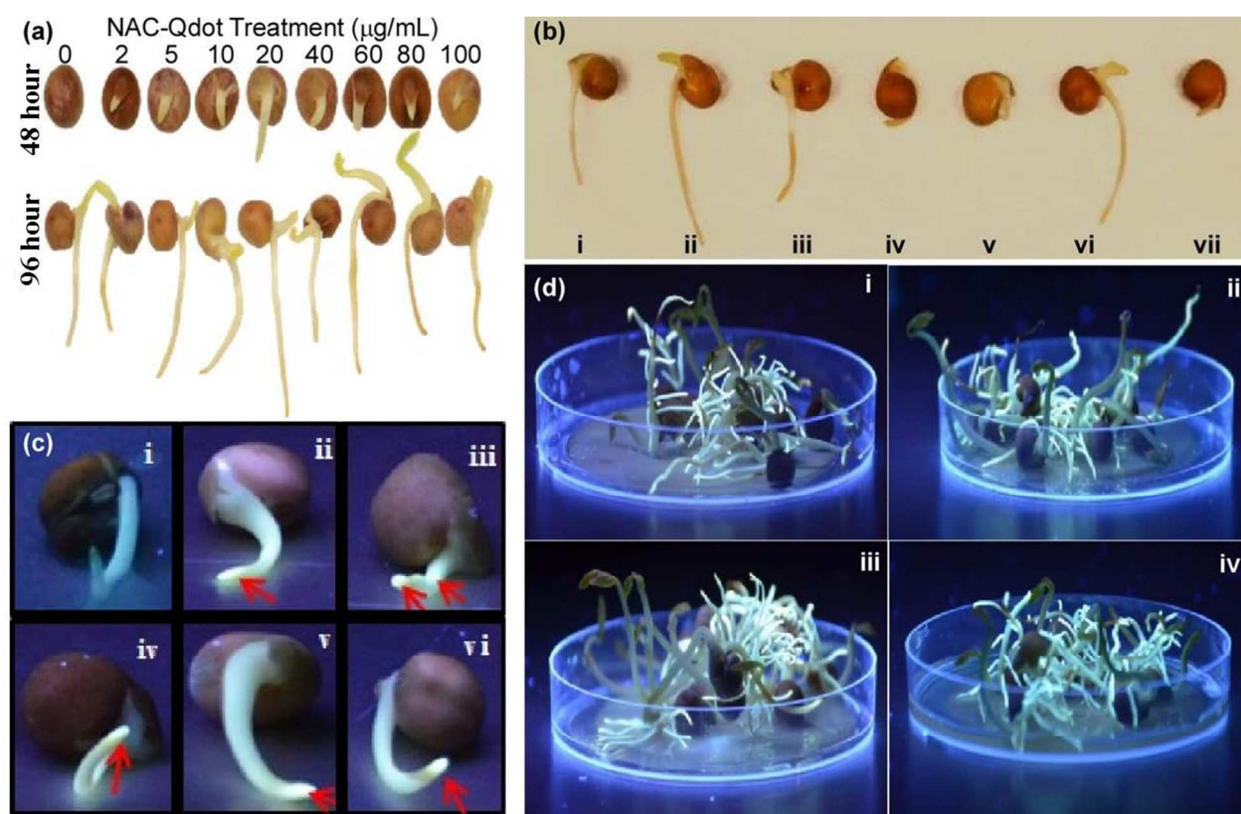


Figure 3. Digital photographs showing the effects of various chemical agents on seed germination of pea (*Pisum sativum*). (a) dose-dependent NAC-Qdot treatment from 0 to 100 µg/mL. (b) isolated materials constitutive of the NAC-Qdots which include DI water (i), NAC + zinc (ii), zinc acetate (iii), cadmium acetate (iv), sodium sulfide (v), NAC (vi) and AOT (vii). (c) Fluorescence response of the germinated seeds: untreated seed showing only background blue auto-fluorescence (i) whereas 2-day treated seed with NAC-Qdot (ii-vi) showing a combined Qdot emission and auto-fluorescence (appeared brighter than untreated control as pointed with red arrows). (d) 4-day treated seeds (i-iv) with NAC-Qdot showing similar emission as seen in (c, ii-vi). Photographs of seeds in (c) and (d) were taken under exposure of a hand-held UV excitation source (366 nm multi-band).

Figure 4.

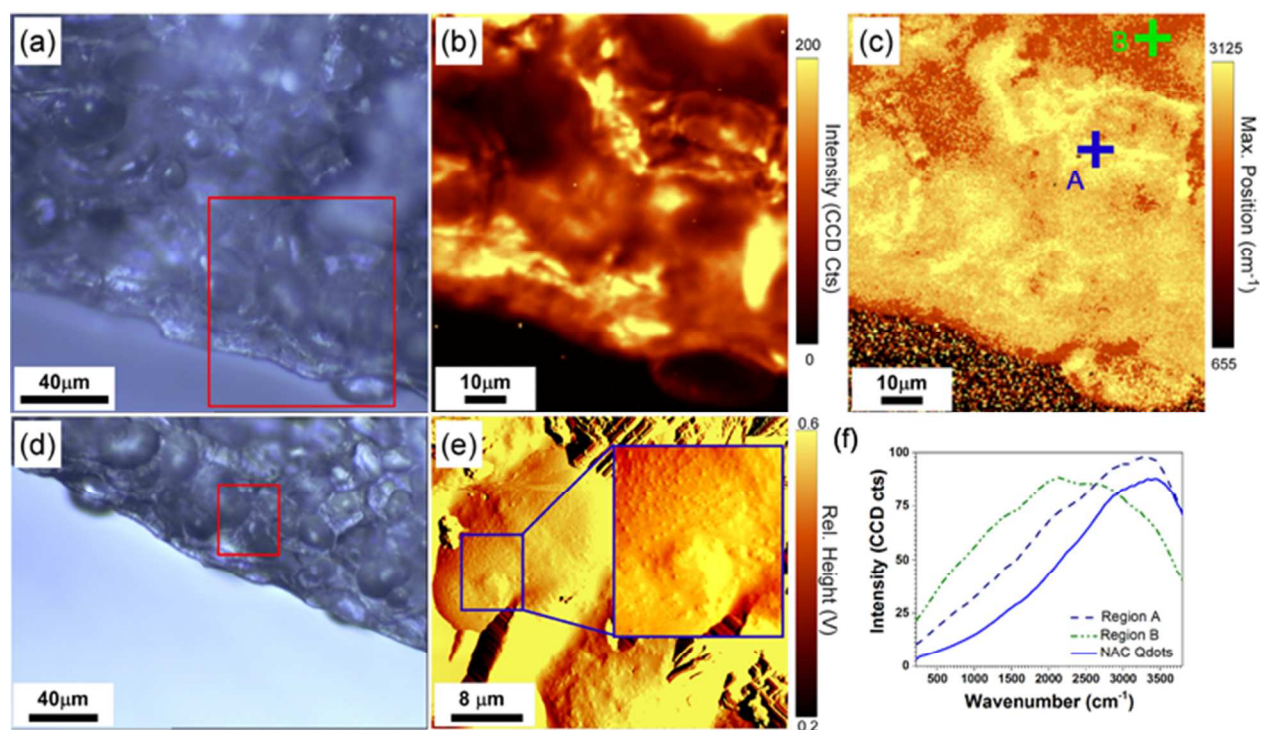


Figure 4. High resolution chemical and topography imaging of seed cells in seed cross section. (a, d) Optical images of the seed cross sections. (b) Raman map representing the intensity of the fluorescence background peak throughout the area in the red box in (a). (c) Raman map representing the position of the fluorescence background peak throughout the area in the red box in (a). Individual Raman spectra obtained at point A and B indicated in (c) and Raman spectrum of the concentrated solution of NAC-Qdots. The data suggest the high concentration of NAC-Qdots in brightest (yellow) areas in (c), for which the position of the maximum peaks was found around 3100 cm^{-1} . (e) High resolution images of the cell tissues obtained with Atomic Force Microscopy (AFM) show the presence of nanoparticle-like structures in regions of the cells with the highest concentration of NAC-Qdots were measured with Raman spectroscopy.

Figure 5.

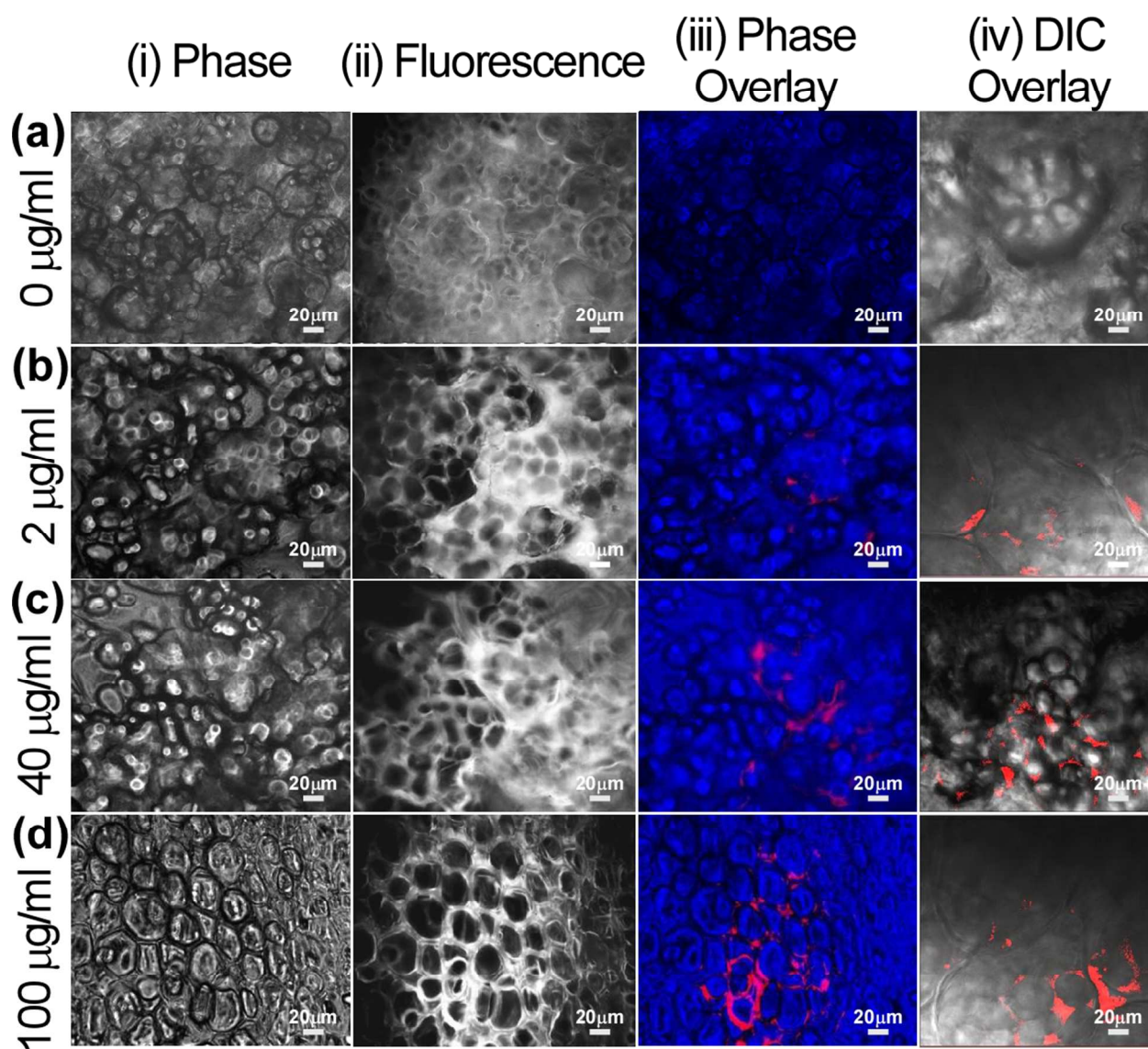


Figure 5. Phase contrast (i), fluorescence (ii), phase-fluorescence overlay (iii) and confocal differential interference contrast (DIC) – fluorescence overlay (iv) images showing absence of quantum dot in untreated seeds (a) and presence of NAC-Qdot quantum dot at the intracellular regions of cells (b-d) of snow pea (*Pisum sativum*)

Figure 6.

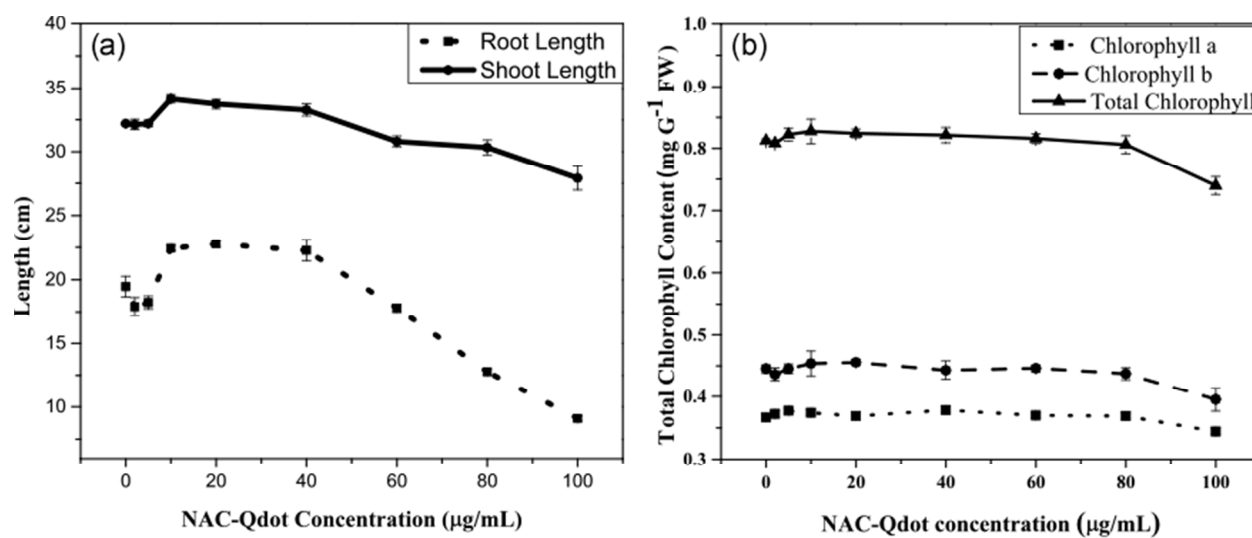


Figure 6. Comparison of (a) root length and shoot length; (b) chlorophyll a, chlorophyll b and total chlorophyll content at different levels of NAC-Qdot based on Duncan test $P \leq 0.05$.